Acta Geologica Sinica (English Edition), 2019, 93(1): 236–237

Research Advances

The Cu-Mo Mineralization of the Late Jurassic Porphyry in the Northern Great Xing'an Range: Constraints from Zircon U-Pb Ages of the Ore-Causative Granites

DENG Changzhou[1, 2, *] and LI Guanghui[2]

[1] *College of Earth Sciences, Jilin University, Changchun 130061, China*
[2] *Heilongjiang Institute of Geological Survey, Harbin 150036, China*

Citation: He et al., 2019. The Cu-Mo Mineralization of the Late Jurassic Porphyry in the Northern Great Xing'an Range: Constraints from Zircon U-Pb Ages of the Ore-Causative Granites. *Acta Geologica Sinica* (English Edition), 93(1): 236–237. DOI: 10.1111/1755-6724.13665

Objective

The Great Xing'an Range (GXAR) is one of the most important metallogenic belts in China. Previous study has shown that porphyry Cu-Mo deposit distributed in the northern Great Xing'an Range formed mainly in two stages: (1) Early Ordovician, such as Duobaoshan and Tongshan deposits (Liu et al., 2017); 2) Triassic-Early Jurassic, including Wunugetushan, Taipingchuan and Badaguan deposits (Tang et al., 2016). In recent years, two potential porphyry Cu-Mo deposits, Huoluotai and Xiaokele, were discovered in the Erguna Block, northern GXAR (Figs. 1a–b). However, the ore formation ages and regional metallogenic regularity are ambiguous due to the lack of isotopic ages. Two zircon U-Pb ages from the ore-causative granites were reported in this paper, with the aims to constrain the metallogenic ages and provide evidence for study of the regional metallogenic regularity and ore prospect prediction.

Methods

Two ore-causative samples, one granodiorite (XLG-30) from the north part of the Xiaokele deposit and one granodiorite porphyry (HLT-1) from the Huoluotai deposit, were collected.

Zircon grains were separated from the study samples by using conventional heavy liquids, magnetic separation techniques, and handpicking under a binocular microscope. Zircon analysis was conducted using the laser ablation inductively coupled plasma mass spectrometry (LA-ICP-MS) at the School of Marine Sciences, Sun Tat-Sen University. Laser sampling was performed using a GeolasPro laser ablation system that consists of a COMPexPro 102 ArF excimer laser (wavelength of 193 nm and maximum energy of 200 mJ) and a MicroLas optical system. An Agilent 7700e ICP-MS instrument was used to acquire ion-signal intensities. Zircon 91500 and glass NIST610 were used as external standards for U-Pb dating calibration, respectively. An Excel-based software ICPMSDataCal was used to perform off-line selection and integration of background and analyzed signals, time-drift correction and quantitative calibration for trace element analysis and U-Pb dating. Concordia diagrams and weighted mean calculations were created using Isoplot/Ex_ver3.

* Corresponding author. E-mail: changzhouhn@126.com

Results

Zircon U-Pb isotopic data are shown in Appendix 1. All the zircon grains are colorless to light gray with oscillatory zonings (Figs. 1c–d). They have high Th/U ratios ranging from 0.62 to 1.53, indicating that they are of igneous origin.

The $^{206}Pb/^{238}Pb$ ages of seventeen zircon grains from granodiorite (XLG-30) range from 147 to 152 Ma, yielding a weighted mean $^{206}Pb/^{238}Pb$ age of 149±1 Ma (MSWD = 0.74; Fig. 1c). Nineteen zircon grains from granodiorite porphyry (HLT-1) yield a weighted mean $^{206}Pb/^{238}Pb$ age of 150±1 Ma (MSWD=1.04; Fig. 1d).

Zircon U-Pb ages of this study suggest a Late Jurassic porphyry Cu-Mo mineralization event in the northern GXAR. Given that the Late Mesozoic magmatism and mineralization in the study area were dominated by the Mongol-Okhotsk Ocean tectonic regime (Deng et al., in press), the generation of the Late Jurassic porphyry Cu-Mo deposits was likely triggered by the southward subduction of the Mongol-Okhotsk Ocean.

Conclusion

Zircon U-Pb ages indicate that the newly discovered Xiaokele and Huoluotai porphyry Cu-Mo deposits formed during the Late Jurassic. The formation of these deposits was probably dominated by the late-stage southward subduction of the Mongol-Okhotsk Ocean, implying that there is a great potential for Late Jurassic porphyry Cu-Mo exploration in the northern GXAR.

Acknowledgements

This research was financially supported by the Land Research Project of Heilongjiang Province (grant No. 201701) and Innovation Fund of Heilongjiang Institute of Geological Survey (grant No. HDDK201806).

References

Deng, C.Z., Sun, D.Y., Han, J.S., Chen, H.Y., Li, G.H., Xiao, B.,

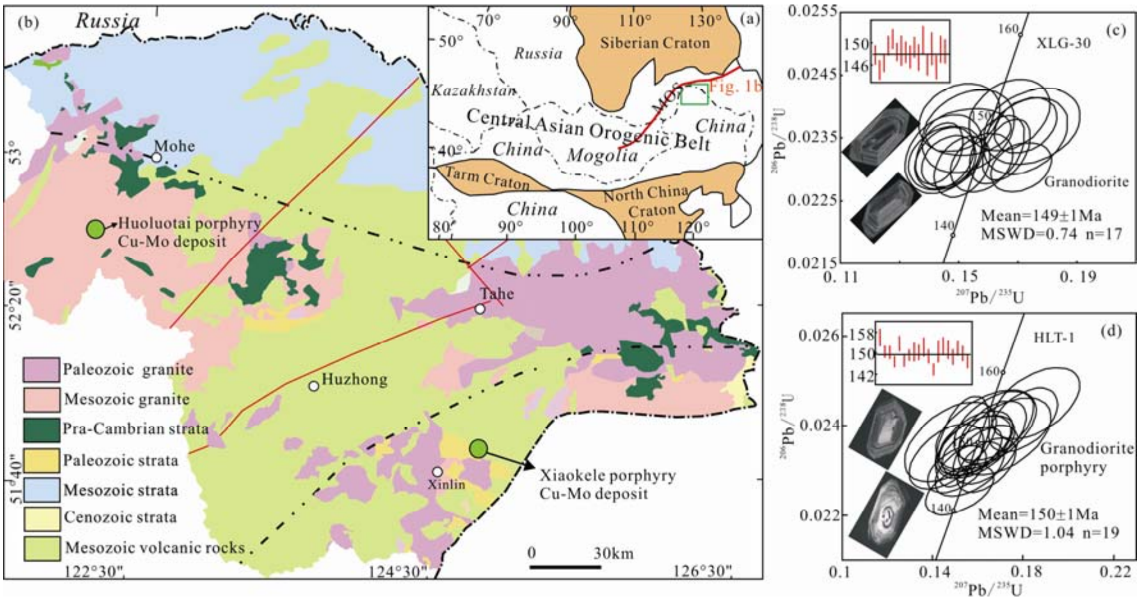

Fig. 1. Geological map of the study area, showing the newly discovered porphyry Cu-Mo deposits, and concordia diagrams of zircon U-Pb ages from the ore-causative granites.

Li, R.C., Feng, Y.Z., Li, C.L., and Lu, S., 2018. Late-stage southwards subduction of the Mongol-Okhotsk oceanic slab and implications for porphyry Cu-Mo mineralization: Constraints from igneous rocks associated with the Fukeshan deposit, NE China. *Lithos*, https://doi.org/10.1016/j.lithos.2018.12.030.

Liu, J., Li, Y., Zhou, Z.H., and Ouyang, H.G., 2017. The Ordovician igneous rocks with high Sr/Y at the Tongshan Prophyry copper deposit, satellite of the Duobaoshan deposit, and their metallogenic role. *Ore Geology Review*, 86: 600–614.

Tang, J., Xu, W.L., Wang, F., Zhao, S., and Wang, W., 2016. Early Mesozoic southward subduction history of the Mongol-Okhotsk oceanic plate: Evidence from geochronology and geochemistry of Early Mesozoic intrusive rocks in the Erguna Massif, NE China. *Gondwana Research*, 31: 218–240.

Appendix 1 Zircon U-Pb data for the ore-causative igneous rocks from the porphyry Cu-Mo deposits in northern GXAR

Analysis spots	Th	U	Th/U	$^{207}Pb/^{235}U$	$^{207}Pb/^{235}U$	$^{206}Pb/^{238}U$	$^{206}Pb/^{238}U$	$^{206}Pb/^{238}U$	$^{206}Pb/^{238}U$	$^{207}Pb/^{235}U$	$^{207}Pb/^{235}U$
	ppm	ppm		Ratio	1σ	Ratio	1σ	Age (Ma)	1σ	Age (Ma)	1σ
Granodiorite porphyry, HLT-1											
HLT-1	205	269	0.76	0.18571	0.01274	0.02451	0.00052	156	3	173	11
HLT-2	252	327	0.77	0.16598	0.01029	0.02364	0.00038	151	2	156	9
HLT-3	224	294	0.76	0.15898	0.01043	0.02359	0.00041	150	3	150	9
HLT-4	551	498	1.11	0.15090	0.00852	0.02303	0.00035	147	2	143	8
HLT-5	609	501	1.22	0.18008	0.00998	0.02413	0.00047	154	3	168	9
HLT-6	573	496	1.16	0.16395	0.00851	0.02312	0.00040	147	3	154	7
HLT-7	543	477	1.14	0.15758	0.00870	0.02343	0.00035	149	2	149	8
HLT-8	164	220	0.75	0.14811	0.01334	0.02364	0.00059	151	4	140	12
HLT-9	284	299	0.95	0.15899	0.01092	0.02360	0.00048	150	3	150	10
HLT-10	97.7	157	0.62	0.16375	0.01458	0.02391	0.00059	152	4	154	13
HLT-11	485	454	1.07	0.16343	0.00939	0.02335	0.00043	149	3	154	8
HLT-12	375	433	0.87	0.15213	0.00995	0.02257	0.00037	144	2	144	9
HLT-13	749	586	1.28	0.15337	0.00783	0.02365	0.00067	151	4	145	7
HLT-14	420	381	1.10	0.16721	0.01162	0.02399	0.00051	153	3	157	10
HLT-16	194	285	0.68	0.17189	0.01351	0.02377	0.00057	151	4	161	12
HLT-17	212	293	0.72	0.14626	0.01084	0.02331	0.00047	149	3	139	10
HLT-18	496	470	1.06	0.16668	0.00979	0.02385	0.00046	152	3	157	9
HLT-19	309	378	0.82	0.15904	0.01139	0.02353	0.00047	150	3	150	10
HLT-20	629	411	1.53	0.15643	0.01005	0.02304	0.00040	147	3	148	9
Granodiorite, XLG-30											
XLG30-1	93	111	0.84	0.15116	0.00621	0.02304	0.00032	147	2	143	5
XLG30-2	79	98	0.81	0.14490	0.00857	0.02324	0.00041	148	3	137	8
XLG30-3	145	147	0.99	0.17107	0.00676	0.02304	0.00026	147	2	160	6
XLG30-5	81	102	0.79	0.17263	0.00696	0.02370	0.00029	151	2	162	6
XLG30-6	124	135	0.92	0.14664	0.00607	0.02313	0.00027	147	2	139	5
XLG30-7	55	76	0.73	0.15320	0.01030	0.02360	0.00044	150	3	145	9
XLG30-8	85	98	0.87	0.15327	0.00954	0.02360	0.00024	150	2	145	8
XLG30-9	66	92	0.72	0.14550	0.00825	0.02318	0.00033	148	2	138	7
XLG30-11	58	83	0.70	0.17262	0.00937	0.02353	0.00040	150	3	162	8
XLG30-12	50	66	0.75	0.17477	0.01075	0.02368	0.00040	151	3	164	9
XLG30-13	91	96	0.94	0.15779	0.00692	0.02311	0.00031	147	2	149	6
XLG30-15	114	122	0.93	0.16615	0.00533	0.02331	0.00032	149	2	156	5
XLG30-16	89	113	0.78	0.14527	0.00657	0.02318	0.00032	148	2	138	6
XLG30-17	78	103	0.76	0.14340	0.00529	0.02325	0.00032	148	2	136	5
XLG30-18	72	96	0.75	0.15022	0.00902	0.02382	0.00036	152	2	142	8
XLG30-19	83	97	0.85	0.16295	0.00609	0.02332	0.00036	149	2	153	5
XLG30-20	63	79	0.79	0.16710	0.00901	0.02386	0.00038	152	2	157	8